Long range surface plasmons in a symmetric graphene system with anisotropic dielectrics

2013 J. Opt. 15 055002

(http://iopscience.iop.org/2040-8986/15/5/055002)

IOP PUBLISHING JOURNAL OF OPTICS
J. Opt. **15** (2013) 055002 (6pp) doi:10.1088/2040-8978/15/5/055002

Long range surface plasmons in a symmetric graphene system with anisotropic dielectrics

K V Sreekanth[1,3] **and Ting Yu**[1,2]

[1] Division of Physics and Applied Physics, School of Physical and Mathematical Sciences, Nanyang Technological University, 21 Nanyang Link, 637371, Singapore
[2] Department of Physics, Faculty of Science, National University of Singapore, 3 Science Drive, 117542, Singapore

E-mail: sxk923@case.edu and yuting@ntu.edu.sg

Received 28 December 2012, accepted for publication 21 February 2013
Published 20 March 2013
Online at stacks.iop.org/JOpt/15/055002

Abstract
We investigate the propagation length of plasmon waves in a graphene film sandwiched by two identical anisotropic dielectrics. The plasmon losses in graphene can be controlled by varying the external carrier doping. In the proposed system, a doped graphene sheet behaves as a thin metal film to support the long range surface plasmons. Here, we consider artificial crystal such as photonic crystal to increase the anisotropy of the dielectrics, which has stronger anisotropy than naturally available optical dielectrics. It is observed that the propagation length, nanoscale mode confinement and penetration depth of surface plasmons increase when the surrounding dielectrics are birefringent crystal with a properly oriented optical axis.

Keywords: graphene, surface plasmons, photonic crystals

(Some figures may appear in colour only in the online journal)

1. Introduction

In recent years, tremendous interest has been generated in the field of graphene photonics and plasmonics [1–7]. Graphene is a single two-dimensional plane of carbon atoms forming a dense honeycomb lattice, enabling the excitation of surface plasmons (SPs) similar to the SPs of metal/dielectric systems. Recent work on graphene plasmonics suggests that surface plasmons in graphene offer potential capabilities for future technological applications [8–15]. However, the plasmon losses must be evaluated and minimized prior to the use of graphene as a potential alternative low loss plasmonic material. Since graphene is a zero bandgap material, the interband transitions (via excitation of electron–hole pairs) contribute large plasmon losses. It has been reported that the plasmon losses in graphene can be controlled by varying the external electrical field and chemical doping [16–20]. Interestingly, graphene behaves like a metal film capable of supporting transverse magnetic (TM) surface plasmons at infrared and THz frequencies when the intraband transitions increase. This is possible when the chemical potential of the graphene is greater than the half of the photon energy. The surface plasmon mode supported by graphene film is considered to be more efficient than surface plasmon polaritons (SPPs), which exist in a homogeneous metal film [21, 22]. It is reported that at 30 THz frequency, the SPP mode guided by free-standing uniformly biased graphene supports a guided wavelength of 144.22 nm, yielding truly nanoscale mode confinement with an effective SPP index of 69.34 [19]. Also, the reported propagation length at the same frequency is 2.25 μm [19]. Note that at the same frequency silver supports a poorly confined SPP mode as well as a higher loss because of the large values of the imaginary and negative real parts of the permittivity. These results show that at THz frequencies (mid-infrared) graphene supports a more highly confined and low loss SPP mode than a noble metal such as silver does at the same frequencies. The major advantages of graphene over noble metal films at

[3] Present address: Department of Physics, Case Western Reserve University, Cleveland OH 44106, USA.

infrared and THz frequencies are (i) the capability to exhibit much larger confinement (volumes 10^6 times smaller than the diffraction limit) and relatively long propagation length, (ii) the capability to dynamically tune the plasmon spectrum of graphene through electrical and chemical doping, and (iii) the capability to achieve SP lifetimes reaching hundreds of optical cycles using highly crystalline graphene samples [19, 20]. In addition, the realization of quantum plasmonics and quantum devices is also expected using graphene plasmonics; these have been difficult to achieve with conventional metal plasmonics to date.

To date, a large number of theoretical studies on the propagation characteristics of surface plasmons along a doped graphene film embedded in symmetric and asymmetric surrounding dielectrics have been performed [23–27]. Recently, the optical coupling of plasmon waves between two graphene sheets embedded in symmetric surrounding dielectrics has been studied and investigated for graphene-based high-speed and ultra-compact optoelectronic devices [26]. In addition, Wang *et al* have studied the coupling of surface plasmons in a monolayer graphene sheet array and showed that the coupling of surface plasmons in the individual graphene sheet results in a reduction of the modal wavelength of the surface plasmons in comparison with that of a single graphene sheet [27].

In this paper, we describe the propagation characteristics of surface plasmons in a graphene film sandwiched by two identical (symmetric) anisotropic dielectric crystals. An artificial crystal such as photonic crystal has been considered as a dielectric substrate to increase the anisotropy of the dielectrics, as it has stronger anisotropy than naturally available optical dielectrics. Also, modification of the dispersion law of the surface plasmon is possible, because photonic crystal is a medium with nonlinear dispersion. The proposed configuration can provide tunable plasmonic properties and may increase the efficiency of graphene-based optoelectronic devices.

2. Theoretical analysis

Here, we consider a symmetric configuration in which a doped graphene sheet of thickness Δ is sandwiched by two identical semi-infinite anisotropic dielectrics such as photonic crystal with principal dielectric constants ε_x, ε_y and ε_z. As shown in figure 1, the dielectrics are assumed to be anisotropic in the (x, z) plane and isotropic in the (x, y) plane, i.e. $\varepsilon_x \neq \varepsilon_z$ and $\varepsilon_x = \varepsilon_y$. Hence, the dielectric substrate can be considered as a uniaxial crystal with two orientations of the optical axis such as parallel and perpendicular to the graphene film.

Since graphene supports TM surface plasmons, it has two electric field components, E_x and E_z, and one magnetic field component, H_y. The E_z field is proportional to the H_y field in each of the three media and the E_x field is proportional to the derivative of H_y with respect to z in each of the three media. Here, we assume that the surrounding dielectric layer thickness is very large compared to the graphene thickness. The H_y field distribution of the TM mode in the surrounding dielectrics can be written as

$$H_{y1}(x, z) = A\exp(\mathrm{i}kx - k_{z1}(z - \Delta)), \tag{1}$$

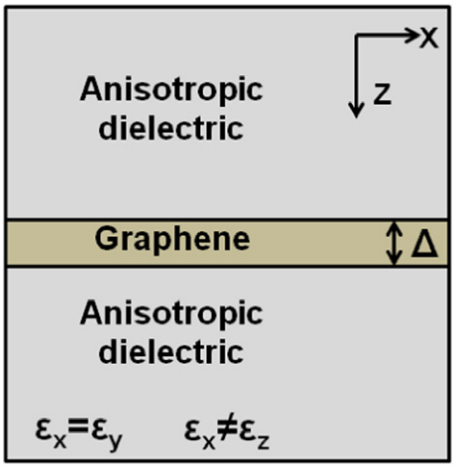

Figure 1. Schematic diagram of the configuration: a doped graphene sheet is sandwiched by two symmetric anisotropic dielectrics.

$$H_{y3}(x, z) = A\exp(\mathrm{i}kx + k_{z3}z), \tag{2}$$

with

$$k_{z1} = k_{z3} = \left(\varepsilon_x\left(\frac{k^2}{\varepsilon_z} - \frac{\omega^2}{c^2}\right)\right)^{1/2}. \tag{3}$$

The H_y field inside the graphene film of thickness Δ can be written as the superposition of two components,

$$H_{y2}(x, z) = B\exp(\mathrm{i}kx + k_{z2}z) + C\exp(\mathrm{i}kx - k_{z2}z), \tag{4}$$

where $k_{z2} = (k^2 - \varepsilon_g\frac{\omega^2}{c^2})^{1/2}$, with the permittivity of the graphene is given by [19]

$$\varepsilon_g = 1 + \mathrm{i}(\sigma_g\eta_0/k_0\Delta), \tag{5}$$

where σ_g is the surface conductivity of graphene, $\eta_0 \approx 377\ \Omega$ is the impedance of air and $k_0 = 2\pi/\lambda$ is the vacuum wavevector with free space wavelength λ.

Since the graphene film occupies the space between $z = 0$ and $z = \Delta$, the requirement of continuity of H_y and E_x at $z = 0$ and $z = \Delta$ gives the dispersion equation for the surface plasmon mode with an antisymmetric distribution of E_x with respect to the plane of symmetry $z = \Delta/2$, which is given by [28]

$$\frac{k_{z2}\varepsilon_g}{k_{z1}\varepsilon_x} = -\tanh\left(\frac{k_{z1}\Delta}{2}\right). \tag{6}$$

Now, it is straightforward to obtain the complex surface plasmon wavevector ($k = k' + \mathrm{i}k''$) of graphene from equation (6), where the real part of the wavevector is related to the speed of the mode and the imaginary part is related to the amplitude attenuation of the mode. Then, the propagation length (L) and effective index (n_{eff}) of the mode are given by $L = 1/2k''$ and $n_{\mathrm{eff}} = k'/k_0$, respectively.

3. Results and discussion

Two different dispersion equations are possible by 90° rotation of the optical axis of the dielectric substrate with respect

to the graphene film. This can be achieved by interchanging the values of ε_x and ε_z. In the theoretical calculation, the principal dielectric permittivities of the photonic crystal are taken to be $\varepsilon_x = 2$ and $\varepsilon_z = 7.5$ for perpendicular orientation and $\varepsilon_x = 7.5$ and $\varepsilon_z = 2$ for parallel orientation. These high dielectric constant values are obtained for a two-dimensional photonic crystal of Si cylinders arranged in a square lattice symmetry at the long-wavelength limit [29]. The dielectric permittivity of graphene is directly obtained from equation (5). Since single layer graphene (SLG) of thickness 1 nm is assumed for the calculation of the complex graphene permittivity using equation (5) [19], here we use an unphysical thickness of 1 nm for the numerical simulations. The surface conductivity of graphene (σ_g) is calculated from the Kubo formula, which is a function of wavelength (λ), temperature (T), momentum relaxation time (τ) and chemical potential (μ_c) [30, 31]. For the calculation of the surface conductivity, we use $\lambda = 10$ μm, $T = 300$ K, $\tau = 0.5$ ps and $\mu_c = 0.15$ eV [24]. The surface plasmon dispersion diagram is shown in figure 2, where the solid (red) and dotted (blue) curves represent the curves for perpendicular and parallel orientation of the optical axis respectively. Moreover, the dispersion curve for an isotropic dielectric (black dashed line) is also shown in figure 2, and lies in between the two orientations. In the case of an isotropic dielectric, the equivalent isotropic dielectric permittivity is assumed to be $\varepsilon_{iso} = \sqrt{\varepsilon_x \varepsilon_z}$.

In order to show the existence of long range surface plasmons in the configuration, the electric field distribution is simulated using the finite difference time domain method (FDTD). The smallest spatial grid size of 0.1 nm is used for the iteration to maintain the accuracy and stability of the FDTD simulations. The incident excitation frequency is assumed to be 30 THz and the dielectric permittivities of photonic crystal are taken as $\varepsilon_x = 2$ and $\varepsilon_z = 7.5$ (perpendicular orientation). The electric field distribution along the (xz) plane of the configuration and the corresponding magnitude along the z-axis are shown in figures 3(a) and (b), respectively. It is evident from the figure that the electric field is mostly confined in the two surrounding anisotropic dielectrics and the field intensity is exponentially decaying (evanescent wave) along the z-direction of these two dielectrics. It should be noted that the field observed in the dielectric medium ($z = 0.45$–0.48) is an artifact due to the field of the incident light source as the light source is placed above the dielectric. Due to the higher refractive index of the surrounding anisotropic dielectrics, these modes have a smaller fraction of the electromagnetic field inside the graphene layer. Hence, the amplitude attenuation is sharply reduced and the propagation length becomes longer.

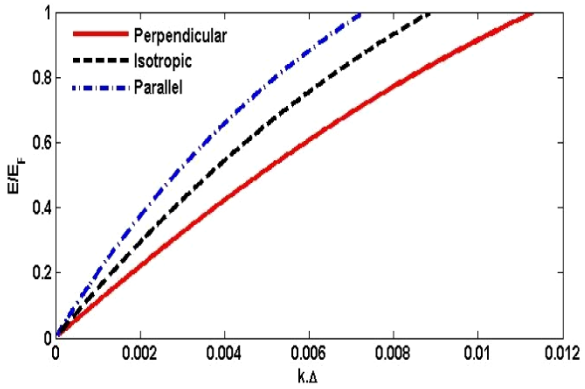

Figure 2. Surface plasmon dispersion diagrams for different orientations of the optical axis of the anisotropic dielectrics. Here, the excitation energy (E) is normalized by the Fermi energy ($E_F = 0.15$ eV) and the wavevector (k) is normalized by the thickness of the graphene (Δ).

The propagation length of surface plasmons for different orientations of the optical axis of the anisotropic dielectric is shown in figure 4. It is clear from the figure that the propagation lengths for three orientations decrease when the excitation energy is increased and the propagation length of a particular orientation reverses at a certain critical excitation energy. The propagation lengths of parallel and

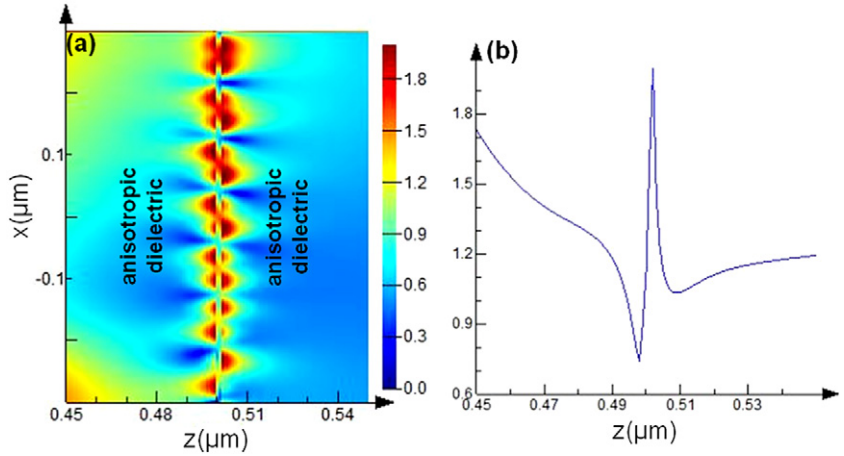

Figure 3. Electric field distributions along the z-direction of the configuration: (a) electric field distribution in the (xz) plane and (b) its magnitude as a function of depth along the z-axis at $x = -0.25$.

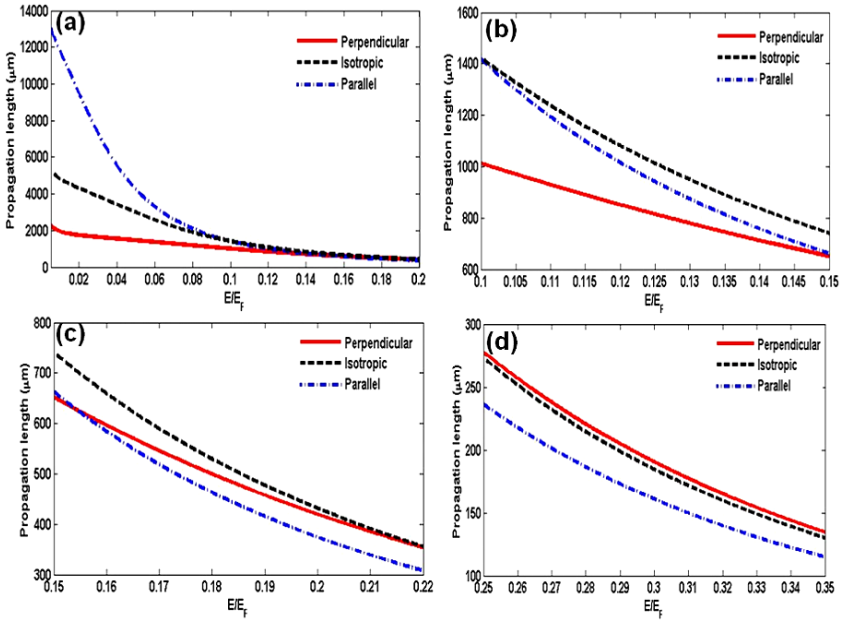

Figure 4. The propagation length of surface plasmons for different orientations of the optical axis of the anisotropic dielectric at various excitation energies: (a) $E/E_F = 0$–0.2, (b) $E/E_F = 0.1$–0.15, (c) $E/E_F = 0.15$–0.22 and (d) $E/E_F = 0.22$–0.35.

perpendicular orientations dominate for lower and higher excitation frequencies, respectively. This shows that we are able to control the propagation length of surface plasmons by tuning the orientation of the optical axis of the anisotropic dielectric. Also note that the propagation length of the isotropic dielectric dominates at certain excitation energies. However, the perpendicular orientation could be more preferable for future graphene-based optoelectronic device applications at near infrared frequencies because it can provide the maximum propagation length in that frequency range (figure 4(d)). In addition, the effective indices of the modes for three different orientations are calculated and plotted in figure 5. It is visible from the figure that the effective indices of all three orientations increase when the excitation energy is increased and the effective index of perpendicular orientation is much higher compared to the other two orientations. This means that the perpendicular orientation provides strong nanoscale mode confinement compared to the other two orientations.

The determination of the penetration depth of the plasmon field into the surrounding dielectric substrate is also equally important for many plasmonics applications. This parameter can be expected to find the coupling strength of the plasmon field with other elements such as quantum dots placed below or above the substrate. The penetration depth of the plasmon field is given by $L_z = 1/k_z$, which can be calculated from equation (3). In figure 6, the penetration depth of surface plasmons for three different orientations of the optical axis of the anisotropic dielectric is plotted. The penetration depths of all three orientations decrease when the excitation energy is increased. It is evident from the figure that the penetration depth for perpendicular orientation is much higher compared to the other two orientations. For the case of parallel orientation, the penetration depth at

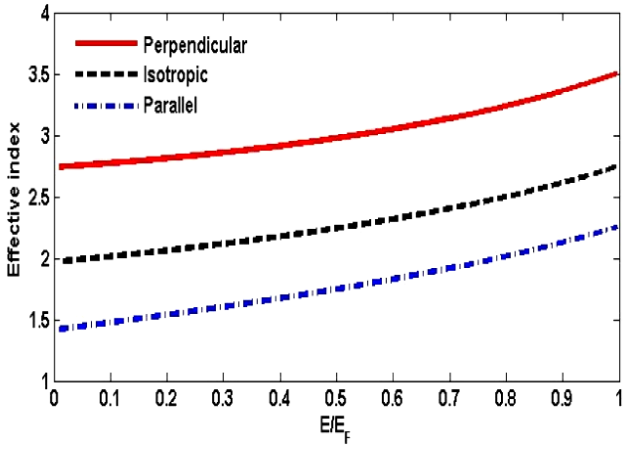

Figure 5. The effective index of the mode as a function of excitation energy for different orientations.

lower frequency is higher than that of an isotropic dielectric. However, at higher frequencies, the penetration depth of an isotropic dielectric is slightly higher compared to that of parallel orientation (figure 6(b)). Hence, it is clear that the penetration depth of surface plasmons can also be controlled by tuning the orientations of the optical axis of the anisotropic dielectric.

For sufficiently large doping of graphene, higher propagation length and longer penetration depth is expected at higher excitation frequencies. Furthermore, the angle-scanned attenuated total reflection method can be used for experimental demonstration of the proposed concept [32]. A narrow dip in the reflectivity versus incident angle plot may give evidence of long range surface plasmon propagation in the configuration. Since large area graphene samples can be widely fabricated using the CVD method, it is feasible

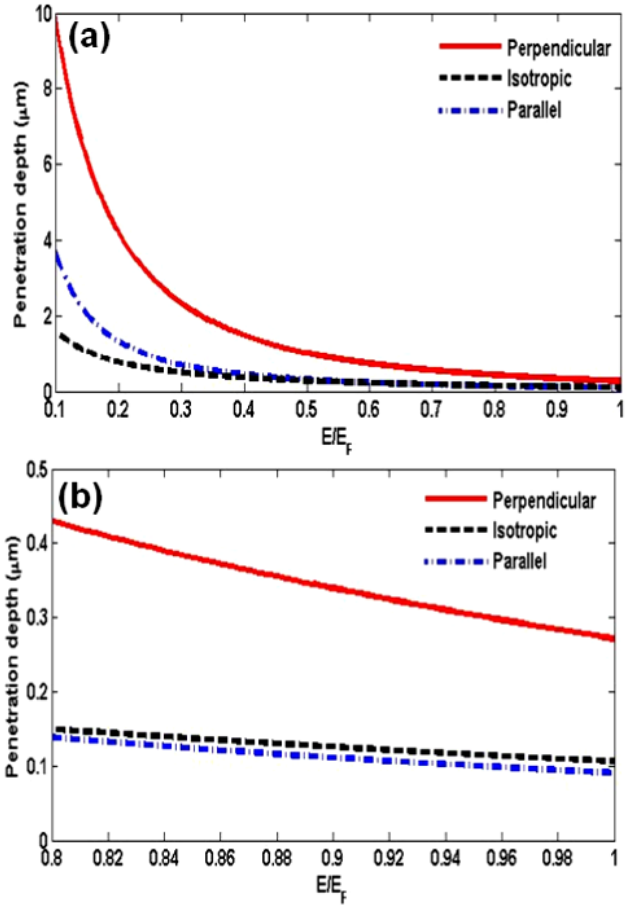

Figure 6. The penetration depth of surface plasmons for different orientations of the optical axis of the anisotropic dielectric at different excitation energies: (a) $E/E_F = 0.1$–1 and (b) $E/E_F = 0.8$–1.

to fabricate the proposed configuration as well [14]. The proposed geometry and concept can be expected to find applications in nonlinear optics and integrated optics for the fabrication of novel graphene-based optoelectronic devices.

4. Conclusion

The existence of long range surface plasmons in a graphene film sandwiched by two identical anisotropic dielectrics at THz frequencies has been investigated. In the proposed configuration, the doped graphene sheet behaves as a very thin metal film to support the long range plasmon waves. The obtained results show that the propagation length and penetration depth of plasmon waves can be controlled when the surrounding dielectrics are birefringent crystal with a properly oriented optical axis. In a wide range of frequencies, the maximum propagation length, stronger nanoscale mode confinement and longer penetration depth are observed for perpendicular orientation. An experimental study is needed to further evidence the proposed concept.

Acknowledgment

The authors acknowledge the financial support received through National Research Foundation NRF RF Award No. NRF-RF2010-07.

References

[1] Bonaccorso F, Sun Z, Hasan T and Ferrari A C 2010 Graphene photonics and optoelectronics *Nature Photon.* **4** 611–22
[2] Grigorenko A N, Polini M and Novoselov K S 2012 Graphene plasmonics *Nature Photon.* **6** 749–58
[3] Tassin P, Koschny T, Kafesaki M and Soukoulis C M 2012 A comparison of graphene, superconductors and metals as conductors for metamaterials and plasmonics *Nature Photon.* **6** 259–64
[4] Sreekanth K V, Zeng S, Shang J, Yong K and Yu T 2012 Excitation of surface electromagnetic waves in a graphene-based Bragg grating *Sci. Rep.* **2** 737
[5] Shang J, Ma L, Li J, Ai W, Yu T and Gurzadyan G G 2012 The origin of fluorescence from graphene oxide *Sci. Rep.* **2** 792
[6] Bao Q and Loh K P 2012 Graphene photonics, plasmonics, and broadband optoelectronic devices *ACS Nano* **6** 3677–94
[7] Cong C, Yu T, Saito R, Dresselhaus G F and Dresselhaus M S 2011 Second-order overtone and combinational Raman modes of graphene layers *ACS Nano* **5** 1600–5
[8] Ju L *et al* 2011 Graphene plasmonics for tunable terahertz metamaterials *Nature Nanotechnol.* **6** 630–4
[9] Wang F, Zhang Y, Tian C, Girit C, Zettl A, Crommie M and Shen Y R 2008 Gate-variable optical transitions in graphene *Science* **320** 206–9
[10] Liu M, Yin X, Ulin-Avila E, Geng B, Zentgraf T, Ju L, Wang F and Zhang X 2011 A graphene-based broadband optical modulator *Nature* **474** 64–7
[11] Mikhailov S A and Ziegler K 2007 New electromagnetic mode in graphene *Phys. Rev. Lett.* **99** 016803
[12] Fei Z *et al* 2012 Gate-tuning of graphene plasmons revealed by infrared nano-imaging *Nature* **487** 82–5
[13] Fei Z *et al* 2011 Infrared nanoscopy of Dirac plasmons at the graphene-SiO_2interface *Nano Lett.* **11** 4701–5
[14] Yan H, Li X, Chandra B, Tulevski G, Wu Y, Freitag M, Zhu W, Avouris P and Xia F 2012 Tunable infrared plasmonic devices using graphene/insulator stacks *Nature Nanotechnol.* **7** 330–4
[15] Chen J *et al* 2012 Optical nano-imaging of gate-tunable graphene plasmons *Nature* **487** 77–81
[16] Wunsch B, Stauber T, Sols F and Guinea F 2006 Dynamical polarization of graphene at finite doping *New J. Phys.* **8** 318–34
[17] Hwang E H and Sarma S D 2007 Dielectric function, screening, and plasmons in two-dimensional graphene *Phys. Rev.* B **75** 205418
[18] Jablan M, Buljan H and Soljačić M 2009 Plasmonics in graphene at infrared frequencies *Phys. Rev.* B **80** 245435
[19] Vakil A and Engheta N 2011 Transformation optics using graphene *Science* **332** 1291–4
[20] Koppens F H L, Chang D E and Garcia de Abajo F J 2011 Graphene plasmonics: a platform for strong light–matter interaction *Nano Lett.* **11** 3370–7
[21] He X Y, Wang Q J and Yu S F 2012 Numerical study of gain-assisted terahertz hybrid plasmonic waveguide *Plasmonics* **7** 571–7
[22] He X Y, Wang Q J and Yu S F 2012 Investigation of multilayer subwavelength metallic–dielectric stratified structures *IEEE J. Quantum Electron.* **48** 1554–9
[23] Rana F 2008 Graphene terahertz plasmon oscillators *IEEE Trans. Nanotechnol.* **7** 91–9
[24] Andersen D R 2010 Graphene-based long-wave infrared TM surface plasmon modulator *J. Opt. Soc. Am.* B **27** 818–23
[25] Gan C H, Chu H S and Li E P 2012 Synthesis of highly confined surface plasmon modes with doped sheets in the midinfrared and terahertz frequencies *Phys. Rev.* B **85** 125431

[26] Wang B, Zhang X, Yuan X and Teng J 2012 Optical coupling of surface plasmons between graphene sheets *Appl. Phys. Lett.* **100** 131111

[27] Wang B, Zhang X, García-Vidal F J, Yuan X and Teng J 2012 Strong coupling of surface plasmon polaritons in monolayer graphene sheet arrays *Phys. Rev. Lett.* **109** 073901

[28] Nagaraj and Krokhin A A 2010 Long-range surface plasmons in dielectric–metal–dielectric structure with highly anisotropic substrates *Phys. Rev.* B **81** 085426

[29] Halevi P, Krokhin A A and Arriaga J 1999 Photonic crystal optics and homogenization of 2D periodic composites *Phys. Rev. Lett.* **82** 719–22

[30] Gusynin V, Sharapov S and Carbotte J 2007 Magneto-optical conductivity in graphene *J. Phys.: Condens. Matter* **19** 026222

[31] Chen P Y and Alu A 2011 Atomically thin surface cloak using graphene monolayers *ACS Nano* **5** 5855–63

[32] Sarid D 1981 Long-range surface-plasma waves on very thin metal films *Phys. Rev. Lett.* **47** 1927–30